

ISSN 0035-3612

M EUROPEAN JOURNAL OF
ECHANICAL
AND ENVIRONMENTAL
ENGINEERING

CONTENTS

Experimental Numerical Analysis Enhancement of Heat Transfer in a Horizontal Circular Tube using Mesh Inserts in Turbulent Region
S.Naga Sarada, A.V.Sita Rama Raju , K.Kalyani Radha

Dynamic Tooth Loads of Helical Gear Transmissions with Higher Gear Ratio
V.Atanasiu, I.Doroftei, C. Rozmarin

About the Evaluation of Electromagnetic Perturbations Generated by Electronic Converters in Robotics
T.Zouaghi, I.Mzoughi, A. Mhamdi



EUROPEAN JOURNAL OF
MECHANICAL
AND ENVIRONMENTAL
ENGINEERING

BSMEE – Belgian Society of Mechanical and Environmental Engineering
2 Rue Hobbemastraat B 1000 Brussels, Tel 32-2-7376553, Fax 32-2-7376547
E-mail : Kristof.harri@rma.ac.be, www.bsmee.be, www.eneest.eu

Aims and Scope of the Journal

The European journal of Mechanical and Environmental Engineering welcomes papers on all aspects of mechanical engineering. Topics include, but are not limited to, machine elements, machine construction, manufacturing technology, tribology, vibrations, environmental testing engineering, mechanical power engineering, mechanical and thermal energy conversion, heat and fluid flow engineering. The journal also

accepts papers of interdisciplinary nature, for example mechatronics, robotics, electronic and optical methods in mechanical and production engineering. The journal especially welcomes papers on environmental engineering, i.e. on the influences of environmental factors on systems or on the interaction of systems with their environment, including security and safety aspects. Essential

for acceptance is however that mechanical engineering forms the core of a submitted paper.

Editorial Board

Chairman

Prof. Y. Baudoïn, Royal Military Academy (BE)

Editor

Dr Ir K. Harri, BSMEE Secretary

Members

Prof JC Samin, Université Catholique de Louvain-La-Neuve
Prof P. Kool, Vrije Universiteit Brussel

Prof S. Vanlanduit, Vrije Universiteit Brussel
Prof B. Lauwers, Katholieke Universiteit Leuven
Prof O. Verlinden, Faculté Polytechnique de Mons
Prof P. Dehombreux, Faculté Polytechnique de Mons
Prof B. Donnay, ISIL, Liège

Scientific Committee

Prof C. Bostater, Florida Institute of Technology
Prof B. Kiss, Budapest University of Technology
Prof I. Doroftei, Technical University of Iasi
A. Charki, LASQUO-ISTIA, France
Prof G. Muscatto, University of Catania
Prof R. Molino, Genova University
Prof M. Armada, CSIC-IAI, Madrid
Prof P. Kopacek, HUT Vienna
Prof M. Maly, ME Institute of Technical University, Liberec
Dr Karl-Friedrich Ziegahn, Forschungszentrum Karlsruhe
Prof B.-R. Höhn, TU München

Prof K. Berns, University of Kaiserslautern
Prof P. Regtien, University, Twente
Prof A. Maslowski, Technical University Warschau
Prof V. Gradetski, Institute for Problems in Mechanics, Moscow
Prof. Håkan Torstensson, CEEES, Sweden
Prof JC Golinval, Université de Liège
Prof E. Dick, Université Gent
Prof R. Van den Braembussche, Von Karman Institute
Prof A. Winfield, University of Bristol

Responsible Editor

Kristof HARRI

Experimental Numerical Analysis Enhancement of Heat Transfer in a Horizontal Circular Tube using Mesh Inserts in Turbulent Region

S.Naga Sarada^a, A.V.Sita Rama Raju^a, K.Kalyani Radha^{*a},

^aDepartment of Mechanical Engineering, JNTUH College of Engineering,
Kukatpally, Hyderabad-500085, Andhra Pradesh, India, Asia.

*Email: kalyaniradha@gmail.com

Abstract

The present work focuses on experimental and numerical investigations of the augmentation of turbulent flow heat transfer in a horizontal circular tube by means of mesh inserts with air as the working fluid. Sixteen types of mesh inserts with screen diameters of 22mm, 18mm, 14mm and 10mm for varying distance between the screens of 50mm, 100mm, 150mm and 200mm in the porosity range of 99.73 to 99.98 were considered for experimentation. The horizontal tube was subjected to constant and uniform heat flux. The Reynolds number varied from 7000 to 14000. The results are compared with the clear flow case when no porous material was used. CFD techniques were also employed to perform optimization analysis of the mesh inserts. The horizontal tube along with mesh inserts was modeled in Gambit 2.2.30 with fine meshing and analyzed using FLUENT 6.2.16. CFD analysis was performed initially for plain tube and the results are compared with experimental values for validation.

Keywords: Enhancement, mesh inserts, heat transfer, turbulent flow, CFD analysis.

1. Introduction

In the recent years, considerable emphasis has been placed on the development of various augmented heat transfer surfaces and devices. This can be seen from the exponential increase in world technical literature published in heat transfer augmentation devices, growing patents and hundreds of manufacturers offering products ranging from enhanced tubes to entire thermal systems incorporating enhancement technology. Energy and material saving considerations, space considerations as well as economic incentives have led to the increased efforts aimed at producing more efficient heat exchanger equipment through the augmentation of heat transfer. Among many techniques investigated for augmentation of heat transfer rates inside circular tubes, a wide range of inserts have been utilized, particularly when turbulent flow is considered. The inserts studied included twisted tape inserts, coil wire inserts, brush inserts, mesh inserts, strip inserts etc. Mesh inserts have a large surface area per unit volume and a much stronger radiation emittance than gas media does, much more energy is emitted by the porous segments mainly back to the upstream direction and cause the temperature to drop sharply along the flow direction. Due to this, porous materials like

mesh inserts have found important applications in high temperature thermal energy systems, where the convection and radiation modes of heat transfer are both important. The utilization of porous inserts has proved to be very promising in heat transfer augmentation. One of the important porous media characteristics is represented by an extensive contact surface between solid and fluid surfaces. The extensive contact surface enhances the internal heat exchange between the phases and consequently results in an increased thermal diffusivity. Different types of porous materials are extensively studied in forced convection heat transfer due to the wide range of potential engineering applications such as electronic cooling, drying processes, solid matrix heat exchangers, heat pipe, enhanced recovery of petroleum reservoirs etc. however the experimental work carried out in this area is limited.

Mehmet Sozen and T M Kuzay [1] numerically studied the enhanced heat transfer in round tubes filled with rolled copper mesh at Reynolds number range of 5000-19,000. With water as the energy transport fluid and the tube being subjected to uniform heat flux, they reported up to ten fold increase in heat transfer coefficient with brazed porous inserts relative to plain tube at the expense of highly increased pressure drop.

Liao. Q and M.D.Xin [2] carried out experiments to study the heat transfer and friction characteristics for water, ethylene glycol and ISOVG46 turbine oil flowing inside four tubes with three dimensional internal extended surfaces and copper continuous or segmented twisted tape inserts within Prandtl number range from 5.5 to 590 and Reynolds numbers from 80 to 50,000. They found that for laminar flow of VG46 turbine oil, the average Stanton number could be enhanced up to 5.8times with friction factor increase of 6.5fold compared to plain tube. Devarakonda Angirasa [3] performed experiments that proved augmentation of heat transfer by using metallic fibrous materials with two different porosities namely 97% and 93%. The experiments were carried out for different Reynolds numbers (17,000-29,000) and power inputs (3.7 and 9.2 W). The improvement in the average Nusselt number was about 3-6 times in comparison with the case when no porous material was used. Fu et al [4] experimentally demonstrated that a channel filled with high conductivity porous material subjected to oscillating flow is a new and effective method of cooling electronic devices. The experimental investigations of Hsieh and Liu [5] report that Nusselt numbers were between four and two times the bare values at low Re and high Re respectively.

Bogdan and Abdulmajeed [6] experimentally investigated the effect of metallic porous inserts in a pipe subjected to constant and uniform heat flux at a Reynolds number range of 1000-4500. The maximum increase in the length-averaged Nu number of about 5.2 times in comparison with the clear flow case and a highest pressure drop of 64.8Pa were reported with a porous medium fully filling the pipe. Paisarn Naphon [7] had experimentally investigated the heat transfer characteristics and the pressure drop in horizontal double pipes with twisted tape insert. The results obtained from the tube with twisted insert are compared with those with out twisted tape.

Betul Ayhan Sarac and Bali [8] conducted experiments to investigate heat transfer and pressure drop characteristics of a decaying swirl flow by the insertion of vortex generators in a horizontal pipe at Reynolds numbers ranging from 5000 to 30000. They observed that the Nusselt number increases ranging from 18% to 163% compared to smooth pipe. Experimental investigation on heat transfer and friction factor characteristics of circular tube fitted with right-left helical screw inserts of equal length and unequal length of different twist ratios was done by Sivashanmugam and Nagarajan [9]. They observed that heat transfer coefficient enhancement for right left helical screw inserts is higher than that for straight helical twist for a given twist ratio. Helical screw

inserts obtained a maximum performance ratio of 2.97. Heat transfer, friction factor and enhancement efficiency characteristics in a circular tube fitted with conical ring turbulators and a twisted-tape swirl generator were investigated experimentally by Promvonge and Eiamsa-ard [10]. Air was used as test fluid. Reynolds number varied from 6000 to 26000. The average heat transfer rates from using both the conical-ring and twisted tape for twist ratios 3.75 and 7.5 respectively are found to be 367% and 350% over the plain tube. The effect of two tube inserts wire coil and wire mesh on the heat transfer enhancement, pressure drop and mineral salts fouling mitigation in tube of a heat exchanger were investigated experimentally by Pahlavanzadeh et al [11] with water as working fluid. The heat transfer rate averagely increased by 22-28% for wire coil and 163 -174% for wire mesh over a plain tube value depending on the type of tube insert, density of wire torsion and flow velocity. Pressure drop also increased substantially by 46% for wire coil and 500% for wire mesh.

Naga .S Sarada et al [12] carried out CFD analysis to investigate the enhancement of heat transfer by incorporating different wire coil inserts in a tube of length 610 mm with an inside diameter of 27 mm. The analysis was performed with air as working fluid for the plain tube and the heat transfer coefficient obtained is compared with the experimental results for validation. It is observed that the heat transfer coefficient obtained analytically is 10.7% more than that obtained experimentally. The Reynolds number ranged from 10353 to 12395. The heat transfer coefficient is found to increase by 190.6% and 311% with wire coil inserts of wire diameter 2.0mm and 3.4mm respectively for a coil pitch of 22 mm when compared with bare tube at $Re = 12395$.

Bogdan and Abdulmajeed et al [13] numerically investigated the effect of metallic porous materials, inserted in a pipe, on the rate of heat transfer. The pipe is subjected to a constant and uniform heat flux. The effects of porosity, porous material diameter and thermal conductivity as well as Reynolds number on the heat transfer rate and pressure drop are investigated. The results are compared with the clear flow case where no porous material was used. The results obtained lead to the conclusion that higher heat transfer rates can be achieved using porous inserts at the expense of a reasonable pressure drop.

The present experimental and numerical study investigates the increase in the heat transfer rate between a pipe heated with a constant uniform heat flux with air flowing inside it when different porous media are emplaced in the core of the pipe. As per the available literature, the enhancement of heat transfer using porous inserts in turbulent region is limited. So, the present work has been done similar lines of Bogdan and Abdulmajeed [13] but in turbulent region (Re number range of 7,000-14,000) as most of the flow problems in industrial heat exchangers involve turbulent flow region.

2. Experimental Work:

2.1 Experimental Setup:

The apparatus consists of a blower unit fitted with a pipe, which is connected to the test section located in horizontal orientation. Nichrome bend heater encloses the test section to a length of a 40 cm. Four thermocouples T2, T3, T4 and T5 at a distance of 5 cm, 15 cm, 25 cm and 35cm from the origin of the heating zone are embedded on the walls of the tube and two thermocouples are placed in the air stream, one at the entrance (T1)

and the other at the exit (T6) of the test section to measure the temperature of flowing air as shown in Figure 1.

The pipe system consist a valve, which controls the airflow rate through it and an orifice meter to find the volume flow rate of air through the system. The diameter of the orifice being 1.4cm and coefficient of discharge 0.64. The two pressure tapings of the orifice meter are connected to a water U-tube manometer to indicate the pressure difference between them. Input to heater is given through dimmer stat. The inner tube of the heating part, which is the test tube with inside diameter 27.5mm, is made of 3.2mm thick copper plate. Display unit consists of voltmeter, ammeter and temperature indicator. The circuit was designed for a load voltage of 0-220V, with a maximum current of 10A. Difference in the levels of manometer fluid represents the variations in the flow rate of air. The velocity of airflow in the tube is measured with the help of orifice plate and the water manometer fitted on board.

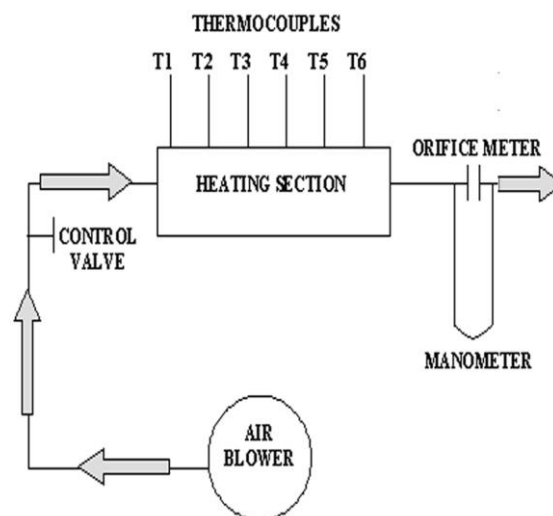


FIGURE 1: EXPERIMENTAL SETUP LAYOUT

2.2 Procedure:

Supply is given to the blower motor and the valve is opened slightly. A heat input of 40W is given to the nichrome heating wire wound on the test section by adjusting the dimmer stat. Thermocouples 2 to 5 are fixed on the test surface and thermocouples 1 to 6 are fixed inside the pipe. The readings of the thermocouples are observed every 5 minutes until they show constant values. Under steady state condition, the readings of all the six thermocouples are recorded. The experiment is repeated for different openings of the valve, thus varying the airflow rate. The fluid properties were calculated as the average between the inlet and the outlet bulk temperature. It took 90 minutes to reach steady state conditions. Experiment was carried out at constant heat flux conditions and constant heat input of 40 W at different mass flow rates, with and without mesh inserts.

2.3 Sequence of Operations:

Experiments are carried out first without inserts and then with inserts.

2.3.1 Without Inserts:

Initially the experiment was carried out without any insert (plain tube experiment). The working fluid air flows through the pipe section with least resistance.

2.3.2 With Inserts:

The porous media used for the experiments are Copper screens as shown in Figure 2 (wire diameter 0.28 mm) cut out at various diameters (D_i) and then inserted on copper rods. That is, 16 different inserts were obtained by varying the screen diameter and the distance between two adjacent screens (p). Thermocouple readings from T1 to T6 are taken for all the mesh inserts shown in Table 1. Each insert is taken and inserted into the test section axially. It is taken care that the strip doesn't scratch the inner wall of the pipe and get deformed.

The presence of the insert in the pipe causes resistance to flow and increases turbulence. The mass flow rates of air and the heat input are same as that of plain tube experiment.

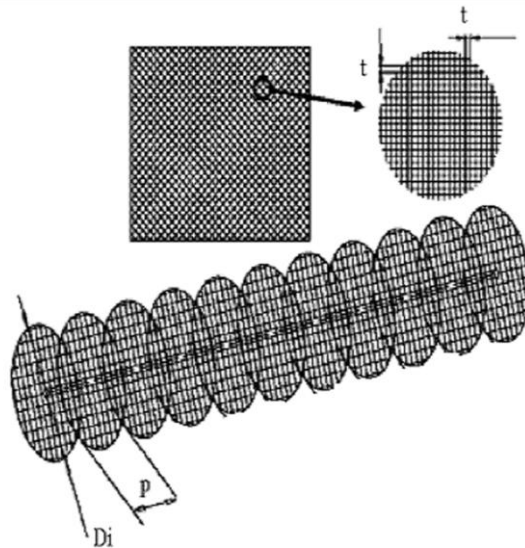


FIGURE 2: POROUS MEDIUM MANUFACTURED FROM COPPER SCREENS

2.3.3 Experimental Uncertainty:

Experiments were conducted initially for plain tube without inserts for 2, 3, 4 and 5 inch water column difference indicated in U-tube water manometer (with mass flow rate of air 0.0047 to 0.0055 kg/sec). The Nusselt number obtained from experimental work is compared with the value obtained using Dittus-Boelter equation (theoretical) (Figure 8). The experimental uncertainty is found as 10% for Nusselt number

2.4 Heat Transfer Calculations:

$$T_s = (T_2 + T_3 + T_4 + T_5)/4 \quad (1)$$

$$T_b = (T_1 + T_6)/2 \quad (2)$$

Equivalent height of air column,

$$h_{air} = (\rho_w * h_w) / \rho_a \quad (3)$$

Discharge of air,

$$d = C_d A_p A_o \sqrt{(2gh_{air})} / \sqrt{(A_p^2 - A_o^2)} \quad (4)$$

$$\text{Velocity of air flow, } U = d/A_p \text{ m/sec} \quad (5)$$

$$\text{Reynolds number, } Re = U D / \nu \quad (6)$$

(To calculate Re while using mesh inserts, D_h instead of D is used)

$$Q = m * C_p * (T_1 - T_6) \quad (7)$$

$$Q_r = \sigma * A * \epsilon_c * (T_s^4 - T_b^4) \quad (8)$$

$$h = (Q - Q_r) / (A (T_s - T_b)) \quad (9)$$

$$Nu = h D / K \quad (10)$$

Eq. (10) gives experimental Nusselt number.

Nusselt numbers calculated from the experimental data for plain tube were compared with the correlation recommended by Dittus-Boelter

$$Nu = 0.023 Re^{0.8} Pr^{0.4} \quad (11)$$

Eq. (11) gives theoretical Nusselt number.

The local values for Nu, Pr and Re were calculated on the basis of air properties corresponding to bulk fluid temperature.

$$f_{the} = 0.25 * [1.82 * \log Re^{-1.64}]^{-2} \quad (12)$$

$$f_{CFD} = (\Delta P * 2 * D) / (\rho_a * L * U^2) \quad (13)$$

Eq. (12) and (13) give friction factor and pressure drop for air passing through test section for plain tube

$$n = (\pi * D_i^2 / 4) / (w + t)^2 \quad (14)$$

$$A_{fr} = [n * w^2 * (\pi / 4 * (D^2 - D_i^2))] \quad (15)$$

$$\epsilon = \text{Void volume} / \text{total volume} \quad (16)$$

$$K = (m * \mu L) / \rho * A_r * \Delta P \quad (17)$$

$$\xi = K_p / L \quad (18)$$

$$\eta = (Nu_i / Nu) / (f_i / f)^{(1/3)} \quad (19)$$

3. CFD Analysis:

There are many devices and systems that are very difficult to prototype. Using CFD analysis, we can predict the performance of a design and test many variations until an optimal result is obtained. To achieve these in physical proto typing and testing would require a huge amount of time and labor. The foresight gained from CFD analysis helps

to design better and faster. The flow inside tube with different types of inserts is characterized by a complex flow field, which is affected by blockage and recirculation zones enhanced by sharp edges. In this case the actual physical device is replaced by a discrete number of points that represent the entire geometry of the cell where the distributions of pressure, velocity etc. are to be found. The approach requires defining the mathematical equations that govern the physical process. These equations will be solved only at the discrete points representing the geometry. CFD techniques are used to perform the overall performance and optimization analysis of the tubes with/without inserts. The fluid flow and heat transfer of the horizontal tube were simulated using FLUENT. The parameters considered for simulation are same as the physical existing parameters for experimental set up like inner diameter of tube 27.5mm, length 61cm, tube and insert materials: copper, heating section 40cm for plain tube etc.

The simulated CFD analysis results like Nusselt number and heat transfer coefficient are validated with the available experimental results for tube with/with out mesh inserts. For completely filling mesh with small pitches like 2.5mm and 10mm and for 26mm mesh diameter ($R_p = 0.9645$), experimental results could not be obtained due to high resistance offered to air flow. Hence those results are obtained through CFD analysis.

Test section geometry is created for all the inserts shown in Table 1 using Gambit. In addition to the mesh inserts shown in Table 1, CFD analysis is extended to 2.5mm pitch and 10mm pitch for screen (mesh) diameters of 26mm, 22mm, 18mm, 14mm and 10mm. As we could not perform the experiments with inserts for low pitches like 2.5 and 10mm the results are obtained through CFD analysis. For 2.5mm pitch and 10mm pitch, number of screens (meshes) in the test section is 244 and 61 respectively.

Boundary conditions used are mass inlet and pressure out let with constant heat flux of 938.96W/m^2 . Each case was run using second order upwind schemes for each governing equation. It was ensured that residuals dropped to at least 10^{-6} for each case.

Mesh is created in 2-D taking symmetric model of the test section. For solution of the problem, segregated solver is used with default settings: implicit formulation, steady (time- independent) calculation, turbulent (k- ϵ model) and energy equation. We used PRESTO as pressure interpolation scheme, SIMPLE as the pressure-velocity coupling method and Second- Order Upwind scheme for density and momentum equations. For under-relaxation factors and convergence criterion were used default values. The solution reached convergence after approximately 1000 iterations. The graphical results are obtained using post process features of FLUENT.

3.1 Heat Transfer Measurements:

The energy equation that FLUENT solves numerically for fluid side has both convective and conductive terms, and the influence of conductive terms on the surface wall temperature values could also be significant. The conduction acts in parallel with convection. Constant wall heat flux is given to check the variation of the temperature over the tube. The difference in the wall temperature and axial fluid temperature ranges from 320K at the starting of the tube to 357.64K at the end of the tube. The exit temperature on the external wall for bare tube $T_s=357.647\text{K}$.

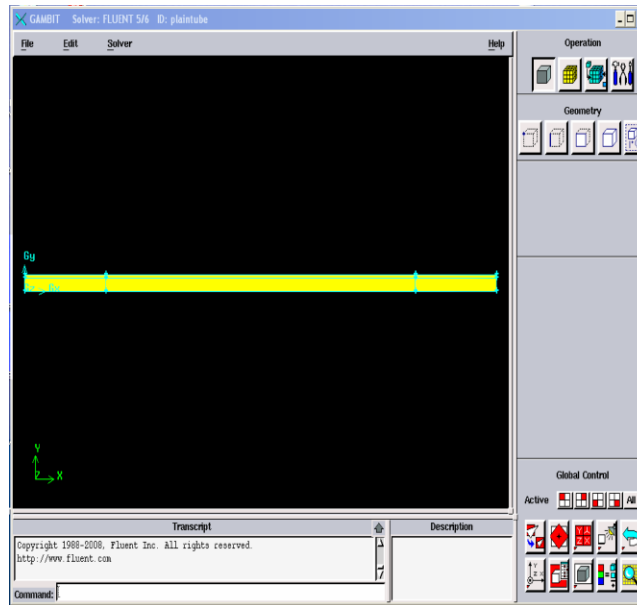


FIGURE 3: GEOMETRIC MODEL FOR PLAIN TUBE CONFIGURATION

Figure 3 shows the model generated in GAMBIT for the horizontal tube with out mesh insert. Mesh is created by taking symmetric model in Gambit (2-D).



FIGURE 4. GEOMETRIC MODEL FOR THE TUBE WITH MESH INSERT (10MM MESH DIAMETER AND 2.5MM PITCH)

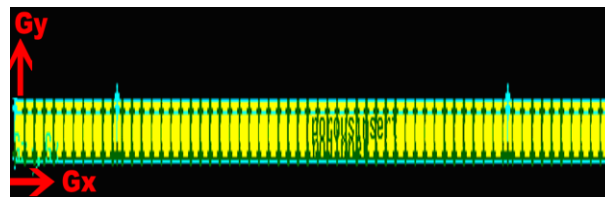


FIGURE 5: GEOMETRIC MODEL FOR THE TUBE WITH MESH INSERT (22MM MESH DIAMETER AND 2.5MM PITCH)

Figures 4 and 5 shows the model generated in GAMBIT for the horizontal tube with mesh inserts 10mm and 22mm mesh diameters with 2.5mm pitch.

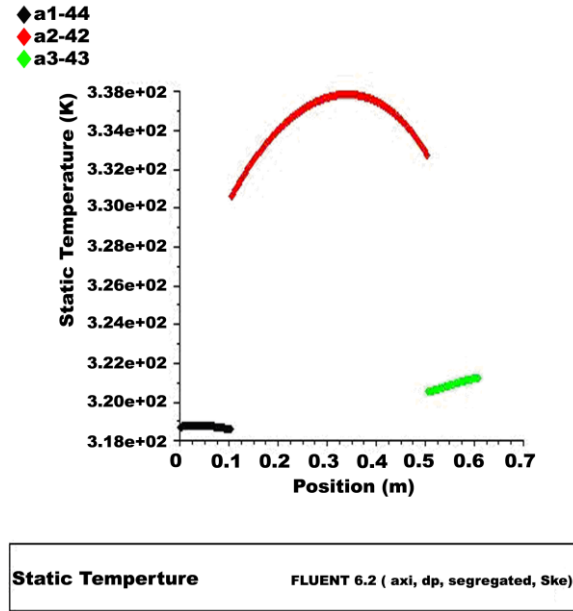


FIGURE 6: TEMPERATURE DISTRIBUTION FOR 10MM MESH DIAMETER WITH 2.5MM PITCH

Figures 6 and 7 show the temperature distribution contours. It can be observed that for the same mesh diameter and mass flow rate of air, tube wall temperature increases with increase in pitch. This is due to less turbulence created for airflow for a comparatively larger pitch (since number of meshes is less for larger pitch). This can be explained by a strong turbulence intensity generated by inserting mesh inserts, leading to rapid mixing of the flow especially at lower pitch diameters.

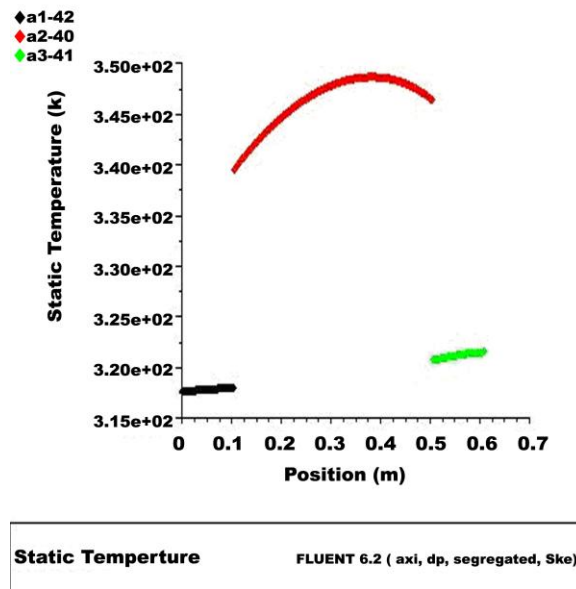


FIGURE 7: TEMPERATURE DISTRIBUTION FOR 10MM MESH DIAMETER WITH 10MM PITCH

4. Results and Discussion:

Experimentally determined Nusselt number values for plain tube (with out mesh insert) are compared with Dittus-Boelter correlation.

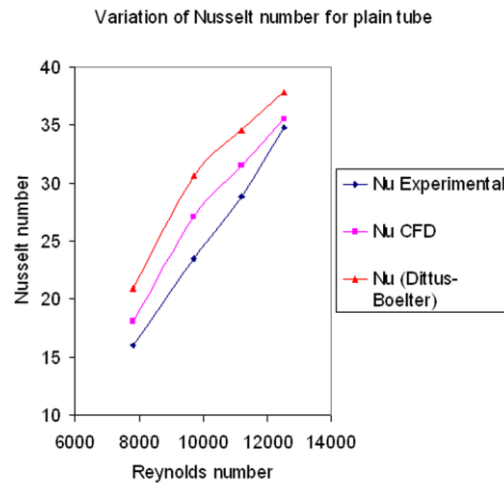


FIGURE 8: COMPARISON OF NUSSELT NUMBER - PLAIN TUBE

Figure 8 shows the comparison between Nusselt numbers obtained experimentally, analytically and by using Dittus-Boelter equation for plain tube. It is observed that Nu (CFD) value is in between Nu (experimental) and Nu (Dittus-Boelter). Actual heat carried away by air passing through the test section is the combination of convective and radiative heat transfers. As the heat transferred by convection alone is considered while performing experimental and numerical calculations (Eq. 8), it can be expected that Nu (experimental) and Nu (CFD) are less than Nu (Dittus-Boelter).

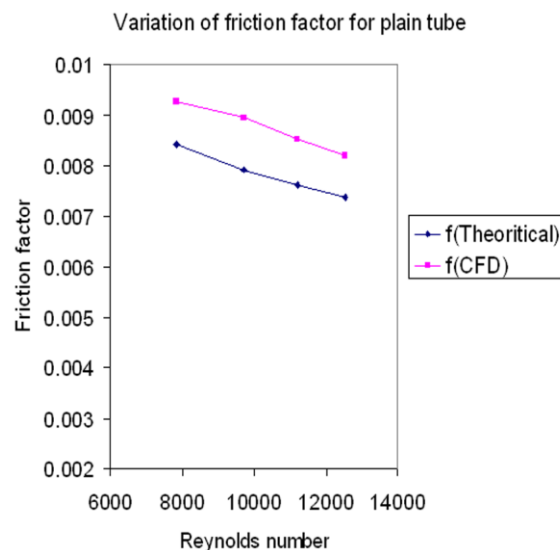


FIGURE 9: COMPARISON OF FRICTION FACTOR - PLAIN TUBE

Figure 9 shows the validation of numerical results for friction factor of plain tube against existing correlation (Eq.10).

Experimental results are summarized in Figure 10. It shows the graph between Nusselt number and Reynolds number for different R_p values obtained experimentally. For the same mass flow rate of air, by keeping R_p constant, the average value of all Nusselt numbers for different pitches 50mm, 100mm, 150mm and 200mm are taken i.e. for R_p 0.8, the average Nu values of mesh insert numbers 1, 2, 3 and 4 as shown in Table 1 are taken for plotting the graph between Re and Nu. Similar procedure is adopted for R_p values of 0.65, 0.5 and 0.364. It is observed that the Nusselt number increased with increase in Re and R_p . This can be expected, as the mesh diameter increased from 10mm to 22mm (R_p 0.364 to 0.8), the obstruction to airflow increases that increases the turbulence created with in the test section. This can be explained by a strong turbulence intensity generated by inserting mesh inserts, leading to rapid mixing of the flow especially at lower pitch diameters. As a result, more heat is carried away by air, which results in increase of Nu. Numerical results are summarized in Figure 11.

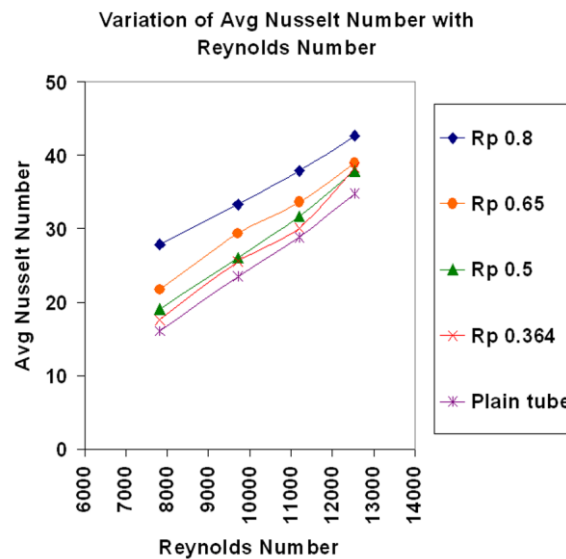


FIGURE 10: NUSSELT NUMBER COMPARATIVE GRAPH WITH AND WITHOUT INSERTS (EXPERIMENTAL)

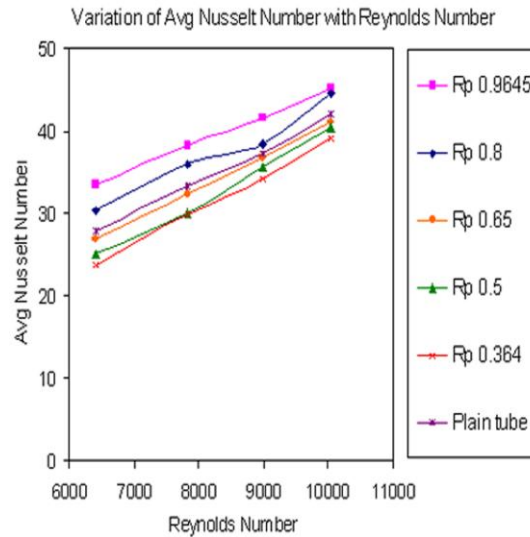


FIGURE 11: NUSSELT NUMBER COMPARATIVE GRAPH WITH AND WITHOUT INSERTS (COMPUTATIONAL)

It shows the graph between Nusselt number and Reynolds number for different Rp values obtained using CFD analysis. It can be observed that, we could obtain Nusselt number for Rp 0.9645 also (in addition to Rp values mentioned in Figure 10) which could not be obtained experimentally as the mass flow rates are proportional to the porous medium’s permeability. For the same mass flow rate of air, by keeping Rp constant, the average value of all Nusselt numbers for different pitches 2.5mm, 10mm, 50mm, 100mm, 150mm and 200mm are taken for plotting the graph between Re and Nu for Rp values of 0.364, 0.5, 0.65, 0.8 and 0.9645. The trend observed is same as Figure 10 with the computational Nu values more than experimental values. It is observed that the Nusselt number obtained by CFD analysis is 15% more than that obtained experimentally.

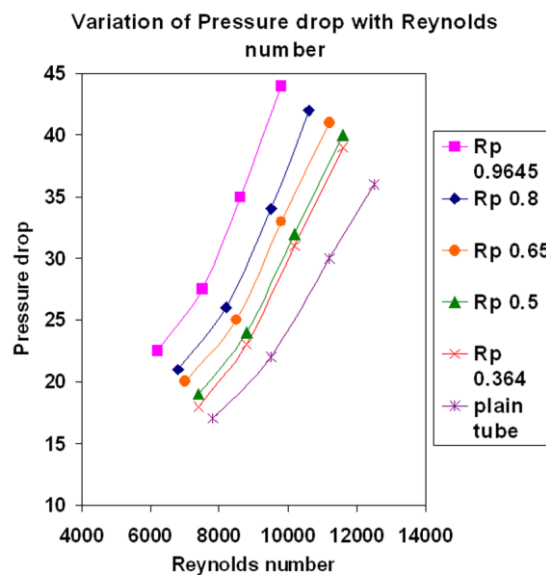


FIGURE 12: PRESSURE DROP VS. REYNOLDS NUMBER

Figure 12 shows the variation of pressure drop with Reynolds number. Pressure drop increases with increase in Reynolds number. Maximum pressure drop is observed to be 1.23 times compared to that of plain tube for insert with $R_p = 0.9645$. The large increase in the pressure drop can be attributed to the tube insert ($R_p = 0.9645$), and the increased velocity associated with a reduced cross-sectional area by tube insert.

Conclusions:

Experimental investigations on enhancement of turbulent flow heat transfer with mesh inserts in a horizontal tube under forced convection with air flowing inside are carried out along with CFD analysis. The variations of temperatures, heat transfer coefficients, Nusselt number in the horizontal tube fitted with various mesh inserts have been studied.

1. The maximum increase in Nusselt number of approximately 1.86 times was obtained through experimental investigation for $R_p = 0.8$ with the distance between screens equal to 50mm. Due to high resistance offered to air flow for mesh inserts with low pitches like 2.5mm and 10mm, experimental results could not be obtained. Hence such results are obtained through CFD analysis.
2. The maximum Nusselt number obtained at smallest pitch (2.5mm) of larger mesh diameter (26mm) using CFD analysis which is 2.15 times that of plain tube.
3. Pressure drop using mesh inserts is found to be maximum for insert with $R_p = 0.9645$ and is 1.23 times compared to that of plain tube.
4. Maximum over all enhancement ratio obtained is 2.006.

For an increase of Nusselt number 2.15 times and pressure drop of only 1.23 times compared to that of plain tube, mesh inserts can be used as a viable alternative compared to other inserts.

References

- [1] Mehmet Sozen and Kuzay, T M., Enhanced heat transfer in round tubes with porous inserts, *Int. J. Heat and Fluid Flow*, April, Vol. 17, (1996) pp. 124-129.
- [2] Liao, Q, Xin, M.D., Augmentation of convective heat transfer inside tubes with three-dimensional internal extended surfaces and twisted-tape inserts, *Chemical Engineering Journal*, Vol. 78, (2000) pp. 95-105.
- [3] Devarakonda Angirasa, Experimental Investigation of Forced Convection Heat Transfer Augmentation with Metallic Porous Materials, *Int. J. Heat Mass Transfer*, May (2001) pp. 919-922.
- [4] Fu, H. L, Leong, K C., Huang, X Y., Liu, C Y., An experimental Study of Heat Transfer of a Porous Channel Subjected to Oscillating Flow, *ASME J. Heat Transfer*, February (2001), Vol. 123, pp. 162-170.
- [5] Shou-Shing Hsieh, Ming-Ho Liu, Huang-Hsiu Tsai, (2003) Turbulent Heat transfer and flow characteristic in a horizontal circular tube with strip-type inserts Part-II (Heat transfer), *International Journal of Heat and Mass Transfer*, Vol 46, pp. 837-849.

- [6] Bogdan, I. Pavel and Abdulmajeed, A. Mohamad, Experimental Investigation of the Potential of Metallic Porous Inserts in Enhancing Forced Convective Heat Transfer, ASME J. Heat Transfer, August (2004), Vol. 126, pp. 540-545.
- [7] Paisarn Naphon Heat transfer and pressure drop in the horizontal double pipes with and without twisted tape insert, International communications in Heat and Mass transfer, Vol. 33, , (2006) pp.166-175.
- [8] Betul Ayhan Sarac and Tulin Bali, An experimental study on heat transfer and pressure drop characteristics of decaying swirl flow through a circular pipe with a vortex generator, Experimental Thermal and Fluid Science, Vol. 32, March (2007), pp. 158-165.
- [9] Sivashanmugam and Nagarajan, Studies on heat transfer and friction factor characteristics of laminar flow through a circular tube fitted with right and left helical screw-tape inserts, Experimental Thermal and Fluid Science, Vol. 32, March (2007), pp.192-197.
- [10] Promvonge and Eiamsa-ard, Heat transfer behaviors in a tube with combined conical-ring and twisted-tape insert, International Communications in Heat and Mass transfer, Vol. 34, May (2007), pp. 849-859.
- [11] Pahlavanzadeh, Jafari Nasr and Mozaffari, Experimental study of thermo-hydraulic and fouling performance of enhanced heat exchangers, International Communications in Heat and Mass transfer, Vol. 34, May (2007), pp. 907-916.
- [12] Bogdan, I. Pavel and Abdulmajeed, A. Mohamad, An experimental and numerical study on heat transfer enhancement for gas heat exchangers fitted with porous media, International Journal of Heat and Mass Transfer, Vol. 47, (2004a) 4939–4952.
- [13] Naga .S Sarada, AV.S Raju and K. Kalyani Radha, Enhancement Of Heat Transfer In Horizontal Tubes With Wire Coil Inserts-A CFD Analysis, International Journal of Applied Research and Engineering, ISSN 0973-4562, Number 9, (2008) pp 1149-1159.
- [14] Frank Kreith, CRC Handbook of Thermal Engineering, CRC Press, Springer Publications (2000).
- [15] Kothandaraman CP and S Subramanyan, Heat and Mass Transfer Data Book, Sixth Edition, New Age International Publishers, New Delhi (2007).
- [16] Pavani .S. Reddy, A CFD analysis of enhancement of heat transfer in a horizontal circular tube using mesh inserts in turbulent region, Master Thesis, JNT University Hyderabad (2008).

Nomenclature

A	convective heat transfer area ($\pi.D.L$), (m^2)
A_0	Area of orifice, (m^2)
A_p	test section inner tube area ($\pi/4 D^2$), (m^2)
A_f	frontal area of porous insert, (m^2)
A_{fr}	free area for air flow, (m^2)
C_p	Specific heat of air, (J/Kg K)

d	air discharge through test section, (m^3/s)
D_i	diameter of mesh insert, (m)
D_h	hydraulic diameter ($4A/P$), m
D	Inner diameter of test section
D_h	hydraulic diameter ($4A/P$)
f	friction factor
f_{the}	friction factor(theoretical)
f_{CFD}	friction factor(numerical)
f_i	friction factor obtained using mesh inserts
h	convective heat transfer coefficient, (W/m^2K)
h_w	manometer level difference,(m)
h_{air}	Equivalent height of air column, (m)
k	thermal conductivity, (W/mK)
K	permeability, (m^2)
K_p	pressure loss factor, ($\Delta P/ \rho_a * U^2$)
L	length of test section, (m)
\dot{m}	mass flow rate of air, (Kg/sec)
n	Number of pores in each mesh insert
Nu	Nusselt number for plain tube, (hD/k)
Nu_i	Nusselt number obtained using mesh inserts, (hD_h/k)
P	wetted perimeter, (m)
p	pitch(Distance between two screens), (m)
Q	total heat transferred to air ($Q_c + Q_r$), (W)
Q_c	heat transferred to air by convection, (W)
Q_r	heat transferred to air by radiation, (W)
Re	Reynolds number, ($\rho u D/\mu$)
R_p	ratio of porous material, (D_i /D)
t	Thickness of the wire mesh, mm
T1, T6	air temperature at inlet and outlet, ($^{\circ}C$)
T2, T3, T4, T5	tube wall temperatures, ($^{\circ}C$)
T_s	average Surface temperature of the working fluid, ($^{\circ}C$)
T_b	bulk temperature, ($^{\circ}C$)
U	air velocity through test section, (m/sec)
w	width of each pore in mesh insert
ε	porosity
ε_c	emissivity of Copper
ΔP	Pressure drop, (Pa)
μ	Dynamic viscosity, (Kg/m s)
η	Overall enhancement ratio
ξ	Inertial resistance factor
u	Kinematic viscosity of air, (m^2/sec)
ρ_w	density of water, (Kg/m^3)
r_p	radius of mesh insert ($D_i/2$), (m)
ρ_a	density of air, (Kg/ m^3)

TABLE 1: MESH INSERT DIAMETERS ALONG WITH DIFFERENT PITCHES

Mesh insert no.	D_i (mm)	p (mm)	R_p	ε (%)
1	22	50	0.8	99.7298
2	22	100	0.8	99.8649
3	22	150	0.8	99.9090
4	22	200	0.8	99.9324
5	18	50	0.65	99.8191
6	18	100	0.65	99.9095
7	18	150	0.65	99.9397
8	18	200	0.65	99.9548
9	14	50	0.5	99.8906
10	14	100	0.5	99.9453
11	14	150	0.5	99.9635
12	14	200	0.5	99.9726
13	10	50	0.364	99.9442
14	10	100	0.364	99.9721
15	10	150	0.364	99.9814
16	10	200	0.364	99.9861

Dynamic Tooth Loads of Helical Gear Transmissions with Higher Gear Ratio

V. Atanasiu, I. Doroftei, C. Rozmarin

Theory of Mechanisms and Robotics Department, "Gh. Asachi" Technical University of Iasi

B-dul D. Mangeron, 61-63, Iasi - 700050, Romania

Email: vatanasi@mail.tuiasi.ro, idorofte@mail.tuiasi.ro

Abstract

In this paper, an analytical formulation is developed to simulate the dynamic load sharing through a mesh cycle of helical gears with a higher gear ratio. The dynamic model is assumed as a single degree of freedom system. A comparative study has been performed to investigate the relation between addendum modification coefficients, mesh stiffness and dynamic load sharing of helical gears. In the analysis, an improved model to calculate the time-varying mesh stiffness of helical gears is presented. The specific geometrical design criteria for the gear pairs are taken into account in these investigations.

Keywords: helical gears, gear ratio, mesh stiffness, dynamic characteristics.

1. Introduction

The increase of the gear ratio of cylindrical gear pairs in the case of a single reduction gearset can be achieved by decreasing the teeth number of the pinion.

There have been several researches on the specific aspects of gear with small number of teeth. Berlinger [4] introduced the concept of high ratio gearing for transmission with small number of pinion teeth and evoloid profile. The combination of single-stage evoloid gears and brushless DC motor was used to ensure a compact actuation-transmission system used for a manipulator structure [8]. Roth and Kollenrott [10] have significantly contributed to the design and manufacturing of gears with small number of teeth and involute profile for tooth module $m_n < 1[\text{mm}]$. Such gear transmissions are usually not used in the power transmission.

Other reported studies focused on the analysis of the specific geometric relationships of helical gears [2, 6, 9] and spur gears [1] with small number of pinion teeth with tooth geometry according to the standard rack and tooth module $m_n > 1[\text{mm}]$.

The dynamic modeling of helical gears with high gear ratio in a single reduction gearset becomes important in order to extend the use of such transmissions for geared servomechanisms.

The accurate evaluation of the load sharing among mesh pairs is one of the major problems in gear design in order to predict the tooth contact pressure, tooth fillet stress, tribological parameters under dynamic conditions. In the paper, the dynamic behavior is quantified on basis of the predicted dynamic meshing loads.

The effect of the time-varying mesh stiffness, one of the main nonlinearities in a geared system on the meshing dynamics, is studied in this paper. An improved analytical model of this parameter is analyzed in order to accurately calculate the cyclic meshing stiffness of helical gear pairs with smaller number of pinion teeth.

The results of the dynamic analysis permit to qualify the design parameters in relation to the magnitude and variation of the contact dynamic loads.

2. Geometrical Design Criteria

At the generating process, the decrease of the number of teeth can be accompanied by the following negative phenomena: tooth undercutting and tooth top sharpening. This negative phenomena reduces the transverse contact ratio and the load capacity

The geometrical criteria are used to prevent the negative phenomena of the generating and engagement processes of helical gears with small number of teeth. Thus, in order to avoid the tooth undercutting, the following condition must be accomplished

$$x_n \geq x_{n\min}$$

(1)

where $x_{n\min}$ represents the minimum value of the addendum modification coefficient to avoid tooth undercutting and can be expressed as

$$x_{n\min} = h_{an}^* - \frac{z \sin^2 \alpha_t}{2 \cos \beta} \quad (2)$$

where z represents the number of pinion teeth, h_{an}^* is the reference addendum coefficient, α_t is the transverse pressure angle and β represents the helix angle. In order to maintain a reasonable value of the tooth thickness s_{an} on the outside circle it is recommended the following condition

$$s_{an} \geq \delta m_n \quad (3)$$

where $\delta = 0.25$ for quenched and tempered steel gears and m_n represents the tooth module.

For a helical gears with a small number of teeth, when Eq. (1) is accomplished but Eq. (2) is not carried out, it is necessary to reduce the whole addendum with a value $\Delta_a m_n$ to avoid tooth top sharpening. In such cases,

$$d_a = m_t z + 2 m_n (h_{an}^* + x_n - \Delta_a) \quad (4)$$

and

$$F(x_n, \Delta_a) = s_{an} - \delta m_n \quad (5)$$

In the design stage it is considered a value $x_n \geq x_{nmin}$ and the Δ_a coefficient is computed on basis of Eq.(5) by using a numerical method. The total contact ratio ε_γ must be always bigger than the unity, in order to preserve the continuity of engagement gears, where

$$\varepsilon_\gamma = \varepsilon_\alpha + \varepsilon_\beta \tag{6}$$

If the transverse contact ratio ε_α results less than the unity, the axial contact ratio ε_β must be established so the total contact ratio ε_γ should became larger than the unity [1].

3. Dynamic Model of a Gear Pair

3.1 Equivalent Line of Action of the Helical Gear Pair

The characteristic of helical gears is mainly involved in the inclination of the contact lines. Both, the position and the length of the contact line at time t have a significant influence on the amount of the mesh stiffness of gears. Therefore, it is necessary to establish these parameters with high accuracy.

Figure 1 shows some of the relevant features of the meshing plane of action for a pair of helical gears. The meshing starts at point A , passes through point E_t and finishes at point E_x . In the analysis it is useful to consider an equivalent line of action AE as shown in Figure 2. The position of the line of contact is indicated with one of the coordinate X or t of the equivalent line of action,

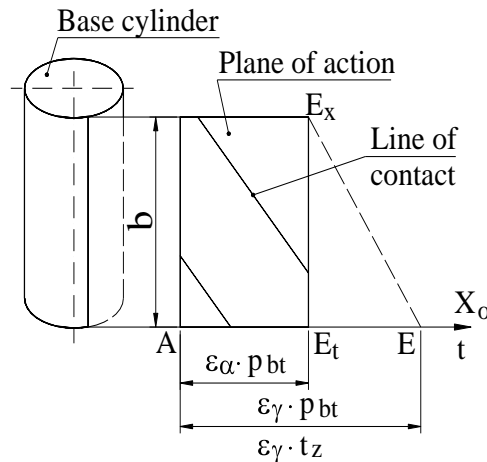


Figure 2: The equivalent line of action of a helical gear

where X shows the meshing position and t is the meshing time:

$$X = X_0 p_{bt}, \quad t = X_0 t_z \tag{7}$$

In the above equations, $X_0 = 0 \sim \varepsilon_\gamma$, and t_z is the meshing time period of passing a transverse base pitch p_{bt} of the helical gears.

3.2 Time varying contact length

For helical gears, the contact length of a tooth pair is not a constant during the engagement cycle. The time-varying of the length of a contact line depends on the ratio between ε_α and ε_β , where ε_α represents the transverse contact ratio and ε_β is the overlap contact ratio. The instantaneous length of a contact line can be expressed as

$$l_c = \frac{\varepsilon_\alpha}{\varepsilon_\beta} \cdot \frac{b}{\cos\beta_b} \cdot c_x \tag{8}$$

where b is the face-width of a gear pair, β_b is the helix angle on the base cylinder, and the parameter $c_x = f(\varepsilon_\alpha, \varepsilon_\beta)$ is shown [].

The total contact length L_c at time t is the sum of the contact lengths of each of the tooth pairs

$$L_c = \sum_{j=1}^N l_{cj} \tag{9}$$

where N is the total number of teeth pairs simultaneously in mesh.

3.3 Dynamic Model

The vibration model for one pair of teeth in contact is shown in Figure 3 . In this model, the teeth are considered as springs and the gear blanks as inertia masses. The transmitted load between the two gears along the normal direction is represented by the static load F_n . The internal forces of the model are the inertia force $m\ddot{x}$, damping force $c\dot{x}$ and the dynamic load F_{di} . The sum of internal forces must be equal to the external force F_n . Hence, the equations of motion can be expressed as

$$m\ddot{x} + c\dot{x} + \sum_{i=1}^N F_{di} = F_n \tag{10}$$

$$F_{di} = k_i y_d + e_i \tag{11}$$

where y_d is the dynamic displacement. The damping coefficient is calculated by

$$c = 2\xi\sqrt{m_e k_m}$$

where m_e represents the equivalent inertia mass and k_m is the average mesh stiffness of the gear pair. For multiple pairs of teeth in contact, the dynamic load is expressed as

$$F_d = \sum_{i=1}^N F_{di} \quad (12)$$

where N represents the number of simultaneous tooth pairs in mesh in the actual position of the gear pairs. The meshing resonance frequency of the gear pair is determined as follows

$$f_n = \frac{1}{2\pi} \sqrt{\frac{k_m}{m}} \quad (13)$$

where m represents the equivalent inertia mass and k_m is the average mesh stiffness of the gear pair.

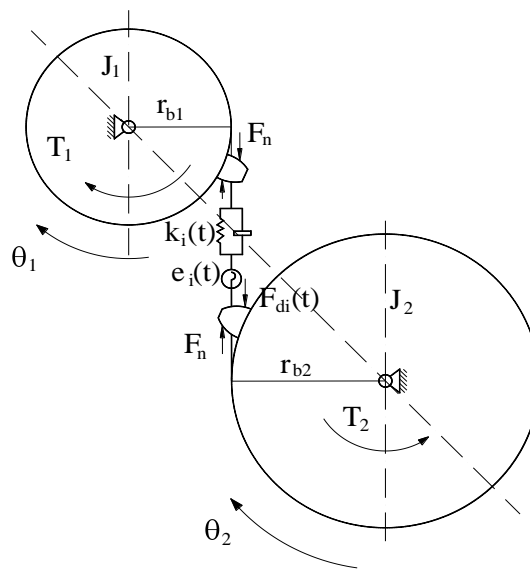


Figure 3: Dynamic model of a spur gear pair

3.4 Time – Varying Mesh Stiffness

The time-varying mesh stiffness represents the main cause of undesired vibrations in the case of gear transmissions with high manufacturing precision. There are few studies on the mesh stiffness the helical gear pairs. Cai [5] presented an approximately stiffness function of helical gears. This model can be used only for helical gears with a standard tooth depth. At the same time, the number of teeth, gear ratio and addendum modification coefficients must be in a specified range geometrical parameters of gear pairs. Therefore, this calculus procedure cannot be extrapolated with good results for other cases, as for helical gears with smaller number of pinion teeth and/or high gear ratio. Other reported studies [7, 11] have assumed a constant mesh stiffness in the dynamic analysis of helical gears.

The deflection f_j of the tooth is defined as the displacement of the point of applied load in the direction of the load. The individual tooth stiffness k_j can be denoted as $k_j = F / f_j$, where F is the normal tooth load per unit length $F = F_n / l_{ci}$. The effects of

bending, shear and Hertzian contact deformation are being taken into account in the analytical method used to calculate the tooth deformation [3].

The mesh stiffness k_i corresponding to a contact line is calculated by using an iterative procedure. Thus, the contact line of a pair of teeth is divided into many equal intervals and k_i is computed as the integral value of the mesh stiffness k_j as it follows

$$k_i = \int_0^{l_c} k_j \cdot dl \tag{14}$$

The teeth pairs in contact act like parallel springs. Therefore, the sum of individual mesh stiffness for all pairs in contact at time t represents the variable mesh stiffness $k_t(t)$ and can be written as

$$k_t = \sum_{i=1}^N k_{ji} \tag{15}$$

where N is the total number of teeth pairs in mesh in the same time. The average value of the mesh stiffness k_m can be expressed as

$$k_m = \frac{1}{t_z} \int_{t_z}^N k_i dt \tag{16}$$

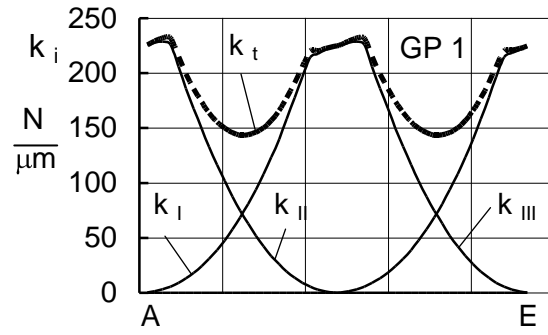
where k_i is the stiffness of the i -th meshing tooth pair.

4. Numerical Results

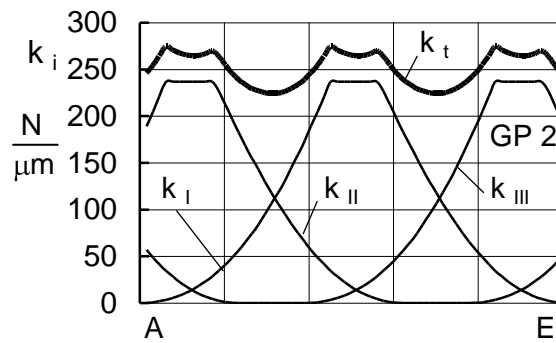
Specifications of the gear pairs which are selected in the analysis are shown in Table 1, where x_{n1} is the addendum modification coefficient of the pinion. These characteristics are for helical gear pairs having tooth module $m=1.5[mm]$, helix angle $\beta=20^\circ$, centre distance $a=90[mm]$, number of pinion teeth $z_1=8$,

Gear pair	x_{n1}	ε_α	ε_β	k_m [N/ μ m]	f_n [Hz]
GP1	0.46*	1.17	0.87	190.1	1710
GP2	0.46*	1.17	1.45	253.6	1597
GP3	0.90	0.99	0.87	146.6	1510
GP4	0.90	0.99	1.45	184.86	1371
* x_{nmin}					

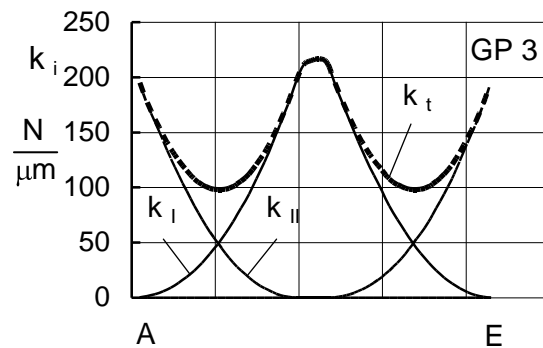
Table 1. Characteristics of the analyzed gears



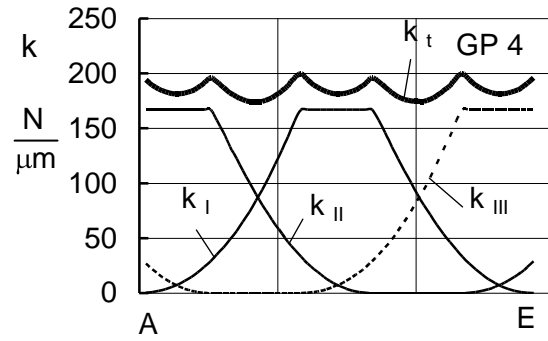
(a)



(b)

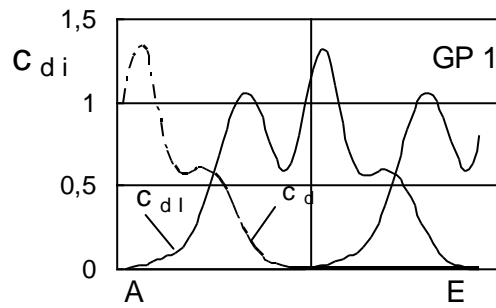


(c)

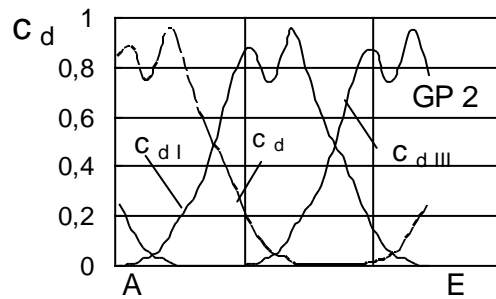


(d)

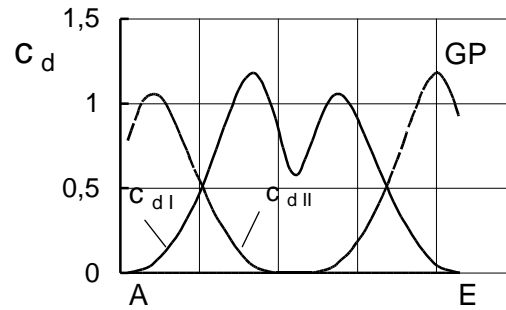
Figure 4: Examples of meshing stiffness of helical gears



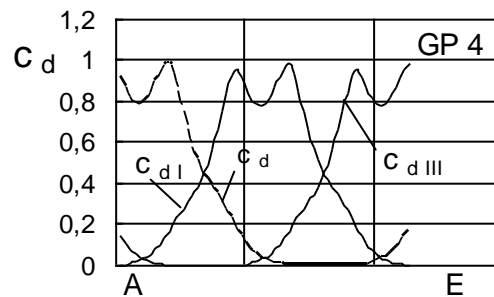
(a)



(b)



(c)



(d)

Figure 5: Variations of dynamic factors

number of gear teeth $z_2 = 102$. Additionally, the design parameters are chosen as: nominal torque, $T_1 = 12[Nm]$; pinion speed, $n_1 = 3400rpm$; damping ratio, $\xi = 0.06$.

For the given centre distance and gear ratio results the sum of addendum modification coefficients as $x_{ns} = x_{n1} + x_{n2}$. The distribution of the sum x_{ns} between pinion and gear allows to change the transverse contact ratio, while the overlap contact ratio is changed by the amount of the tooth face-width. The selected values of the tooth face-width allow to obtain total contact ratios smaller or larger than 2.

A computer program was developed for simulating the dynamic characteristics of helical gear pairs. The equations of motion are solved by the fourth-order Runge-Kutta method.

The results given in Figure 4 show the effects of the total contact ratio and its components on the mesh stiffness variation during a mesh cycle. An increase of the transverse contact ratio has as effect upon the increase of the average mesh stiffness k_m . The mesh stiffness k_m grows up with increasing the overlap contact ratio. The relation between them is nonlinear.

The gear mesh stiffness is dependant on the total contact ratio, while the equivalent inertia mass varies with the overlap contact ratio. At the same time, by varying the tooth face-width on a constant torque, the normal load on the length of line of contact is not a constant. These aspects are specific ones in the analysis of helical gear pairs.

The meshing dynamics of the gear pairs are expressed by the dynamic load factors c_{di} , where c_{di} corresponds to shared dynamic loads on gear teeth pairs. The dynamic factor is defined as the ratio of the dynamic load to the nominal static load transmitted by the

gear pair. It is characterized by the amplitude and its peak to peak value. The dynamic loads are calculated using detailed contact analysis for discrete positions in the meshing cycle. Examples of the variations of the dynamic factors c_{dj} are shown in Figure 5, where $i = I, II, III$ represents the teeth pair in contact.

The time-varying mesh stiffness has a significant effect upon the dynamic factors. As shown in Table 1 and Figs.4 and 5, the gear pairs having a higher average stiffness k_m and a smaller cycling variation have a lower amount and variation of the dynamic factors c_{dj} . The dynamic behavior of helical gear pairs can be improved by increasing the total mesh stiffness.

5. Conclusions

An analytical procedure for calculating the dynamic characteristics of helical gears with smaller number of pinion teeth is presented. This procedure predicts the variation of the individual dynamic factors during the meshing cycle. The specific geometrical design criteria for these gear pairs are taken into account in these investigations.

The effect of contact ratio on dynamic behavior of helical gear pairs was examined by using the mesh stiffness parameter. The time-varying mesh stiffness along the path of contact is found by using an exact analytical model. The total contact ratio and the combination of transverse and overlap contact ratios were found to have a significant influence on the dynamic behavior of helical gear pairs.

The dynamic model takes into account the realistic mesh stiffness and should be used for more accurate control of geared servomechanisms.

Acknowledgements This work was supported by CNCSIS –UEFISCSU, project number 76 PNII – IDEI code 296/2007.

References

- [1] Arikan, M.A.S. Performance Rating and Optimization of Spur Gear Drives with Small Number of Teeth. *Proc. of the 2000ASME Design Engineering Technical Conferences*, September 10-13, Baltimore, Maryland, USA, pp.21-30, 2000.
- [2] V. Atanasiu, Optimum Design of Cylindrical Gears with Smaller Number of Pinion Teeth. *Proc. of the Ninth World Congress on the Theory of Machines and Mechanisms*, Milano, pp.477-481, 1995.
- [3] V., Atanasiu, An Analytical Investigation of the Time-Varying Mesh Stiffness of Helical Gears. *Bul. Inst. Polit. Iasi*, XLIV(XLVIII),1-2, S.V., pp.7-17 (1998).
- [4] B.E. Berlinger. Das Evaloid-Verzahnung-system fur Stirnradgetriebe mit-grossen Stufenubersetzungsverhältnis, *Konstruktion*, 7, 156-158, 1977.
- [5] Y. Cai, Simulation on the Rotational Vibration of Helical gears in Consideration of Tooth Separation Phenomenon (A New Stiffness Function of Helical Involute Tooth Pair). *Journal of Mechanical Design*, Vol.117, pp.460-468, 1995.
- [6] C.F. Chen, C.B. Tsay, Tooth Profile Design for the Manufacture of Helical Gear Sets with Small Number of Teeth, *International Journal of Machine Tools and Manufacture*, 45, pp. 1531 – 1541, 2005.
- [7] He, S., Singh, R. Dynamic Transmission Error Prediction of Helical Gear Pair under Sliding Friction using Floquet Theory. *Journal of Mechanical Design*, Transactions of the ASME, Vol.30, 052603/1-9 (2008).

- [8] R. Holberg, S. Dickert and O. Khatib, A New Actuation System for High-Performance Torque-Controlled Manipulators. *Proc. CISM-IFTOMM Symposium on Theory and Practice of Robotics and Manipulators*, Springer-Verlag Berlin Heidelberg, pp. 285-292, 1993.
- [9] A. Ishibashi, H. Yoshino, I. Nakashima, design, Manufacturing Process and Load Capacity of Cylindrical Gear Pairs with 2 to 4 Pinion Teeth for High Gear Ratio, *Bulletin of the JSME*, Vol. 24, No. 198, pp. 2210-2217, 1981.
- [10] K. Roth and F. Kollenrott, Zahnradpaarungen mit Komplementprofilen zur Erweiterung der Eingriffsverhältnisse und Erhöhung der Fuss- und Flankentragfähigkeit, *Konstruktion* 34, H.3, 81-88, 1982.
- [11] P. Velez, M. Ajmi, Dynamic Tooth Loads and Quasi-Static Transmission Errors in Helical Gear—Approximate Dynamic Factor Formulae. *Mechanism and Machine Theory*, 42, pp. 1512-1526, 2007.





LABORATORY DYNAMICS OF MECHANICAL STRUCTURES



The laboratory is part of the Department of Mechanics of the Royal Military Academy. LDMS is able to perform vibration testing in order to simulate the environmental, mechanical conditions that act on a product or structures. The laboratory can perform a research of resonance frequencies, a sine dwell, a sine sweep, random vibrations and shock tests in accordance with several standards, such as MIL-STD-810, IEC 255-21-2, IEC 60068-2 series,...

The quality of these activities is guaranteed by the ISO-17025 standard and the laboratory is accredited by the Belgian government: BELAC Accreditation certificate 273-TEST. Several international standards are included within our scope:



Cert. 273-T
ISO 17025

MIL-STD-810 E: Method 514.4: Vibration
MIL-STD-810 E: Method 516.4: Shock
MIL-STD-810 F: Method 514.5: Vibration
MIL-STD-810 F: Method 516.5: Shock
IEC 255-21-1
EN 61373
IEC60574-1
IEC 600068-2-series

**Tests that are not covered by our scope are executed with the same level of quality.
An extension of the scope is also possible.**

The laboratory is equipped with modern high-quality hard and software. The main piece is a RMS electro-dynamic shaker with a maximum capacity of 18 kN and able to work vertically as well as horizontally. The vibration control and data acquisition is done by a LMS SCADAS III with 8 channels and by the LMS Test.Lab software.



More information about our laboratory can be found on: www.ldms.rma.ac.be or by contacting us:
 Technical Director: [Professor Baudoin](mailto:yvan.baudoin@rma.ac.be): +32 2 742 6553 or yvan.baudoin@rma.ac.be
 Quality Manager: [K. HARRI, dr. ir.](mailto:kristof.harri@rma.ac.be): +32 2 742 6683 or kristof.harri@rma.ac.be
 Technical Manager: [JF HERBIET, ir.](mailto:jean.francois.herbiet@rma.ac.be): +32 2 742 66 46 or jean.francois.herbiet@rma.ac.be

About the Evaluation of Electromagnetic Perturbations Generated by Electronic Converters in Robotics

T.Zouaghi^{1,3}, I.Mzoughi², A. Mhamdi²

Academy of Fonduk Jedid, Km 29- GP1 – Road of Grombalia -Tunis- Tunisia, e-mail:

t.zouaghi@enit.rnu.tn / zouaghitaoufik@yahoo.fr

Aviation School of BorjElamri, Km 22 – GP4 - Road of Béja – Tunis – Tunisia

Research Laboratory SICISI, ESSTT, 5, Av. T. Hussein, 1008, Tunis, Tunisia

Abstract

Electromagnetic compatibility / electromagnetic interferences (EMC/EMI) filters are widely used in robot sensors and actuators. These machines are usually electronically controlled. The sensitive electronics must be protected from EMC perturbations which can interfere with the process quality and the reliable functioning of the machinery.

The aim of this paper is to carry out an electromagnetic perturbation study of a power converter commutation cell in which perturbation measurement is ensured by means of an impedance stabilizer which is a device to create known impedance on power lines of electrical equipment during electromagnetic interference testing. It ensures two tasks: isolating the device under test from the net on which perturbations of both common and differential modes may occur, and allowing measurements in better conditions. Reduction of the undesirable phenomenon caused by the parasitic elements of electromagnetic perturbations needs to go into the commutation mechanism study of the most simple of power converter structures: a commutation cell. Results of this approach are very interesting and their analysis worth going into.

Keywords: Electromagnetic Compatibility, Power converter, switching cell, Parasitic Coupling, Electromagnetic perturbations, High frequency.

1. Introduction

Technical applications are increasingly equipped with robot cells. The high-frequency interference and electromagnetic perturbations originating from electronic drive units for servomotors, should be limited. The use of EMC/EMI filters and line reactors enables the systems to function reliably and ensures problem-free operation.

With the advent of widespread static converters power supply in the late 20th century and later in the 21st century miniature electronic circuits. As switching devices became commonplace, typically in industry but also in domestic appliances and robotics. From the 1970's, the popularity of modern digital circuitry rapidly grew. As the technology developed, with faster switching speeds (increasing emissions) and lower circuit voltages (increasing susceptibility), EMC increasingly became a source of concern. Many more nations became aware of EMC as a growing problem and issued directives to the manufacturers of digital electronic equipment, which set out the essential

manufacturer requirements before their equipment could be marketed or sold. As switching devices became commonplace especially in machine and actuator drives used in robots, power electronics have considerably increased last decades. They use power semiconductors operating at switching modes which confer to them a high efficiency, but cause many electromagnetic perturbations essentially due to fast switching of semiconductors. These perturbations propagate either to the supply source or to the load circuit. A small part of its energy radiates in the enviroing space. To well approach this phenomenon of electromagnetic compatibility (EMC) in power electronics, the present paper carry out an electromagnetic (EM) study of a commutation cell in which perturbation measurement is ensured by means of impedance stabilizer.

2. The line impedance stabilization network (LISN)

A LISN is a device to create known impedance on power lines of electrical equipment during electromagnetic interference testing. A LISN is typically designed to allow for measurements of the electromagnetic interference existing on the power line. It fulfils three main functions:

- It filters the mains voltage and should block higher frequencies than the mains frequency.
- It should provide characteristic impedance to the device under test (DUT).
- The conducted interference voltage produced by the DUT is transferred to a meter, for example a spectrum analyser or an EMI receiver.

A LISN is basically a very large and effective " π - type" electrical noise filter used in the design and measurement of electronic equipment to meet formal specifications such as the "CE Marking". Its large capacitors and inductors (which would never be used in consumer equipment for safety reasons involving potentially high-current short-circuit current paths!) absorb nearly all unwanted noise energy and essentially "isolate" electrically the Device Under Test ("DUT") from any of the power mains. The LISN is supposed to keep unwanted conducted noise from coming in on the power mains and tainting measurement of the DUT, and it is also supposed to keep noise generated by the DUT from escaping back into the power mains. The purpose is to allow accurate measurement of noise generated by the DUT using, usually, a broadband spectrum analyzer.

The Line Impedance Stabilization Network looks like a filter which is inserted between the device under test and the supply source. It ensures two tasks: isolating the device under test from the net on which perturbations of both common and differential modes may occur, and allowing measures in better conditions. However, the voltage drop (input / output) of the LISN should not exceed 5% of the nominal voltage under the nominal current.

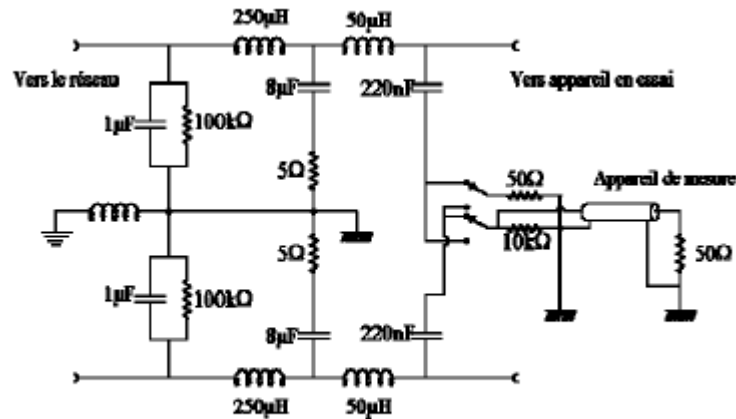


Figure 1: Principle Scheme of one phase LISN

Inductance / capacitance filter allows low frequencies and eliminates the perturbations of the net. Capacitance / resistance filter allows high frequencies into a 50 Ω measuring resistor. The LISN could be utilized for current values rising upon 100A. Beyond this value, a current probe could be also utilized

3. Example of perturbation mechanism: analysis in a switching cell

In the simple case of a switching cell represented in Figure 2, the voltage and current shapes in the switch are considered trapezoidal. Commutation time « τ » either for currents and voltages of a mean calibre MOSFET or IGBT switch, is very short (typically 10 to 100 nanoseconds). Analysis of such a case worth going into as far as it shows that voltage and current quick variations may cause damageable electromagnetic perturbations to the device.

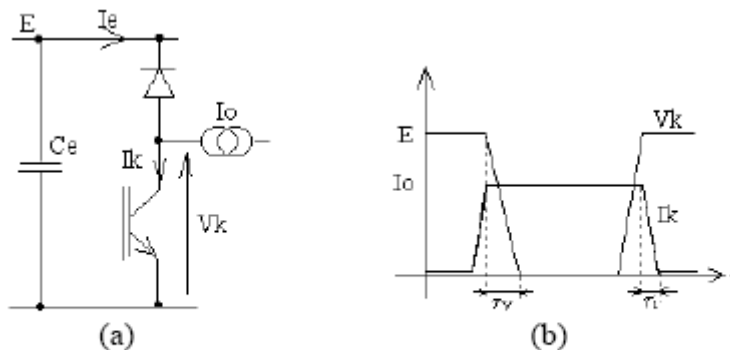


Figure 2 - (a) : Commutation Cell – (b) : Current and Voltage Shapes

Fourier series decomposition of such type of signals which magnitude is A and cyclic ratio is α, is given by equation (1) where HF harmonics are expressed.

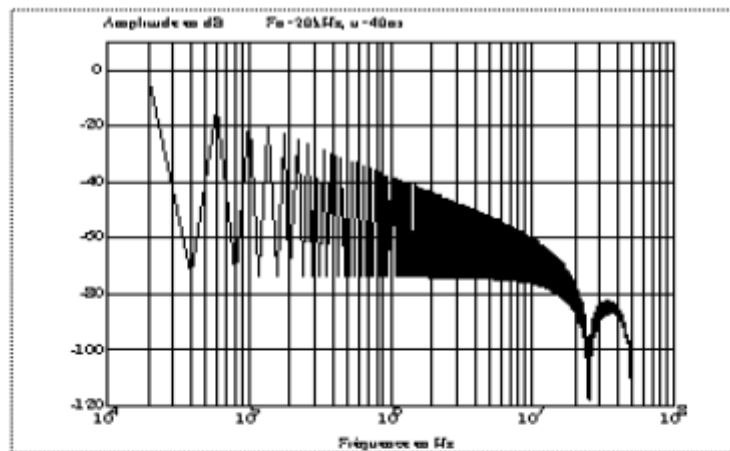
$$A_n = 2A\alpha \frac{\sin(\Pi.n.Fo.\tau)}{\Pi.n.Fo.\tau} \cdot \frac{\sin(\Pi.n.Fo.to)}{\Pi.n.Fo.to} \quad (1)$$

Notice that the envelop of maximums of An is constant as fare as $F < F1=1/to$, then

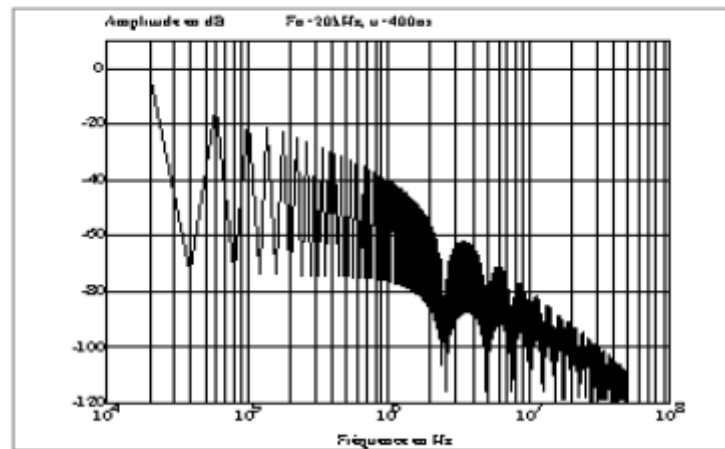
decreases as $1/F$ to $F_2 = 1/\tau$, and decreases again as $1/F^2$. The spectrum is larger and decreasing slowly as τ is small. Figure 3 shows two examples with two values of τ of 40 ns and 400 ns, where t_0 is taken equal to 25 sec., the obtained values of F_2 are respectively 8MHz and $F_2=0.8\text{MHz}$.

Thus, it appears clearly, that the speed of commutations is an important parameter in the occurring mechanism of perturbations. It convenes then, to limit its value for both current and voltage: dV/dt and dI/dt .

We have also noticed that for high levels of dI/dt and dV/dt , perturbations have a large band spectrum with small decrease. So, it would be better to control them while switching, by slowing of the interrupter drive which operates at low frequencies, or by associating soft switching structures with a slow control



(a)



(b)

Figure 3 : Spectral Analysis - (a): Influence of current variations dI/dt – (b): influence of voltage variations dV/dt

3-1. Consequence on the conducted perturbations

Conducted perturbations are transmitted to the enviring devices such as the LISN (RSIL) by way of the various coupling impedances illustrated in Figure.4.

Notice that the high frequency current generated by the commutation cell is shared between capacitance C_e and the impedance R_o of the LISN

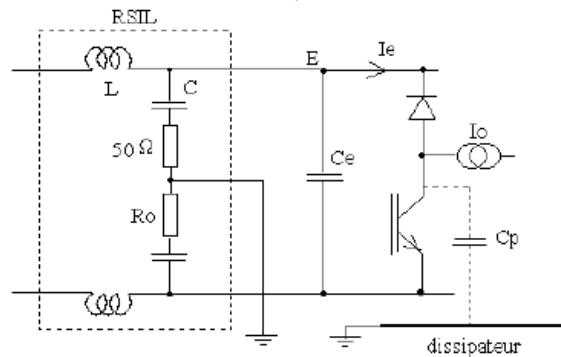


Figure 4: Common and differential mode coupling of perturbations to enviring components

Notice also that imperfections on capacitance C_e may induce the increase of high frequency perturbations.

3-2. parasitic elements of the switching cell

The model with trapezoidal shapes defined in the above is not able to explain pulses of very high frequencies in the parasitic signal spectrum. Their origin remains in the parasitic components of the commutation loop, i.e.: the turned off switch parasitic capacitances and parasitic inductances of cables or the component intrinsic inductances (bonding). They have as effect, the parasitic high frequency resonant signals which accuracy increases with the speed of switching, as far as the commutation lost damping is not sufficient. This is easily remarkable on the simplified model of the commutation cell given by Figure 5. High frequency supplementary harmonics due to resonance are coupled to electric environment by mean of capacitances inducing common mode currents and also by mean of radiations.

Figure 6 and Figure 7 represent voltage and current shapes in the commutation cell, electromagnetic perturbations rise when switcher is blocked. They are measured by the LISN inserted between the supply and the cell. This induces either over voltage (dv/dt) or over current (di/dt) speeds. In our case:

$$\text{- over voltage} = \frac{dv}{dt} = \frac{\Delta v}{\Delta t} = \frac{36}{0,01 \cdot 10^{-5}} \text{ V/S}$$

and,

$$\text{- over current} = \frac{di}{dt} = \frac{\Delta i}{\Delta t} = \frac{3}{0,006 \cdot 10^{-5}} \text{ A/S}$$

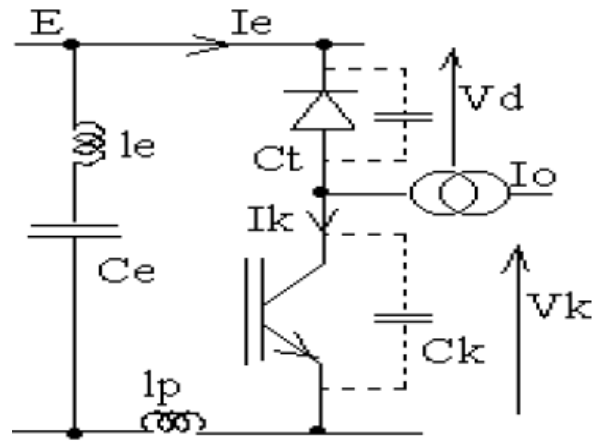


Figure 5 : Switching cell simplified model

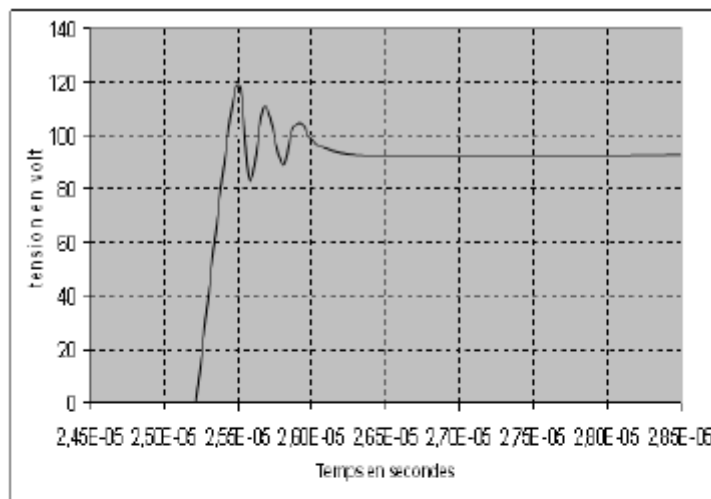


Figure 6: Voltage Shape in the switching cell

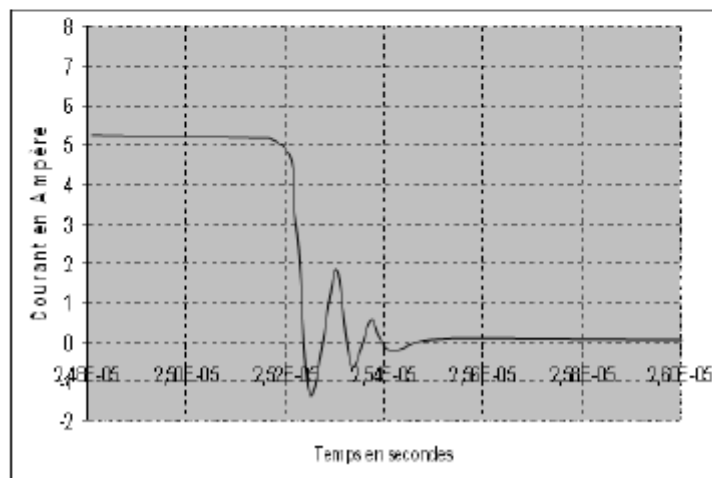


Figure 7 : Current Shape in the switching cell

4. CONCLUSION

The technology behind robots is characterized by complex systems integration. These systems which are compound of mechanical devices, on-board sensors, redundant computer systems and advanced mechatronics must meet stringent requirements for the utmost in operational safety so to ensure smooth and reliable operation of machines and systems switcher high performances of speed and control as well as high frequencies in these devices, have induced power converters widespread all over the energy control domains. The consequence of this development is the increase of global level of EM perturbations. EM pollution seems like a mismanagement of residual energies in static converters coupled to electric environment by means of several parasitic parameters. Reduction of this undesirable phenomenon needs to go into the commutation mechanism study of the most simple of power converter structures (a commutation cell), and then, more complex structures where magnetic components have a major role, could be considered. Soft switching could bring to us a first solution to this problem, but, if we want to decrease the level of perturbations, we should reduce their original sources by means of filtering or minimisation of coupling. Whereas technical specifications are going more and stronger, EMC considerations should have the same importance in the design of equipment, than the other criteria such as efficiency, volume and technical performances. Designer must be aware of this concept to improve the quality of equipments.

References

- [1] F. Wrobel, F. Saigné « Contraintes radiatives associées aux matériaux des composants micro et nanoélectroniques » REE, N°3 – Mars 2010. pp. 33-38.
- [2] J.L. Autran, D. Munteanu, S. Sauze, P. Roche, G. Gaziot and J. Borel « La plateforme astep du plateau de bure – Tests en environnement radiatif de composants et circuits électroniques » , REE, N°3 – Mars 2010. pp.39 – 48
- [3] R.C. Baumann, “ Radiation-induced Soft Errors in Advanced Technologies” IEEE Transactions on Device and Material Reliability. Vol. 5, N°3, pp.305-316
- [4] S. Mita, P. Sanda and N. Seifert “Soft Errors Technology Trends, System Effects and Protection Techniques” IEEE VLSI Test Symposium, 2008.
- [5] A. Puzo, « Contribution à l'étude des perturbations rayonnées dans les convertisseurs haute fréquence », Doctorate thesis of Ecole Centrale de Lyon-jun-2002.
- [6] F. Costa, « Contribution à l'étude des perturbations conduites dans les convertisseurs haute fréquence », Doctorate thesis Université d'Orsay Paris-Sud, April 2002
- [7] W. Ott, « Noise reduction techniques in électronique systèmes », John Wiley and Sons.
- [8] P. Degauque et J. Hamelin, « Compatibilité électromagnétique », éditions Dunod 1999.
- [9] Lu Bei, « Contribution à l'étude du rayonnement en champ électromagnétique proche des circuits en électronique de puissance », Doctorate thesis of Ecole Centrale de Lyon, may 1998.
- [10] J.P. Charles, « Modes de détection en analyse spectrale », technical report NT/PAB/ETR/759 du CNET, november-1997.
- [11] A. Azoulay, J.P. Charles, « Méthodes de mesure de compatibilité électromagnétique », note technique NT/PAB/ETR/693 du CNET, february 1995.
- [12] A. L'Haridon, « Compatibilité électromagnétique dans les systèmes à forte concentration électronique », Techniques de l'Ingénieur E1530.
- [13] J.L. Schanen, J. Roudet, W. Teulings and F. Mérienne, « Modèles analytiques de Prédiction de Performances CEM d'une cellule de commutation MOSFET – Diode »,

- EPF'98 – Belfort. [14]M. d'Armoro, A.Moriello, M.S. Sarto, "ANeural Approach for Identification of EM Field Sources – Analysis of PCB Configurations", IEEE *Trans. On PowerElectronics*–1998.
- [15]Z. Khatir "Simulation des Dispositifs de l'Electronique de Puissance", INRETS Report N° 219, Nov.1997.



Contact Information for the Europe Office:

Jeroen van Liempd, Director of EMEA Operations
Email: vanliempdj@asme.org, Tel: +32 2 740 2227, Fax: +32 2 743 1550

Géraldine Damar, Manager Education programmes and Corporate Solutions
Email: damarg@asme.org, Tel: +32 2 740 2241, Fax: +32 2 743 1550

Bertrand Mbiaffié, Community and Corporate Coordinator
Email: mbiaffieb@asme.org, Tel: +32 2 743 15 43, Fax: +32 2 743 15 50

Mags Rivett, Marketing and Communication Manager
Email: rivettm@asme.org, Tel: +32 2 789 2232, Fax: +32 2 743 1550

Claudia Fortes, Marketing and Communication Manager
Email: fortesc@asme.org, Tel: +32 2 789 2341, Fax: +32 2 743 1550



What we do ...

For your workers : noise and vibrations exposure quantification and contribution analysis

For your environment : noise and vibrations measurements

For your products and processes : Vibro-acoustics studies on machines (design and maintenance)

For you : Training and consciousness-raising



MoDyVA offers consulting services in acoustics and vibrations. Our goal is to help companies having noise and vibrations problems at the workplace and in the environment. We also assist our customers to design less vibrating and more silent products.

You're looking for solutions in vibrations and acoustics ?
Please contact us or visit our website :

 With the support of the Walloon Region

+32 (0)65 37 41 80
+32 (0)476 672 111
philippe.brux@MoDyVA.be
www.MoDyVA.be

c/o Faculté Polytechnique de Mons
Rue de Houdain, 9
B-7000 Mons
BE 882.779.875

renowned and respected for its Codes and Standards, which are in use throughout the world, and also for its technical publications, conferences, and the hundreds of professional development courses that are conducted each year.

ASME Europe

The ASME Europe Office was opened in Brussels in April 2005 to serve members in Europe, Middle East and Africa, and to reach out to the wider European engineering community. A growing network of ASME Sections and student Sections are operating in Europe - offering professional and personal development activities and networking potential.

The ASME Europe Office offers a number of strategic services geared towards engineers in the region.

Contact us to find out how you can benefit from working with ASME.

ASME shapes the engineering community's future through a number of services:

- Codes & Standards
- Publications
- Global Exchange
- Safety and Conformity
- Engineering Advocacy
- Continuing Education / Lifelong Learning
- Volunteers and regional Affiliates
- Engineering achievement
- Global Career Resources



ASME Europe Office
Avenue de Tervueren, 300
B-1150 Brussels
Belgium
Tel: +32 2 743 1543
Email: info-europe@asme.org
Visit: www.asme.org/communities/international/europe